Fabrication of Porous Polyketone Forward Osmosis Membranes Modified with Aromatic Compounds: Improved Pressure Resistance and Low Structural Parameter

Nakagawa, Keizo ; Uchida, Kiyohito ; Wu, Jiang Ling Chuan ; Shintani, Takuji ; Yoshioka, Tomohisa ; Sasaki, Yuji ; Fang, Li-Feng ; Kamio,…

(Citation)
Separation and Purification Technology,251:117400

(Issue Date)
2020-11-15

(Resource Type)
journal article

(Version)
Accepted Manuscript

Fabrication of Porous Polyketone Forward Osmosis Membranes Modified with Aromatic Compounds: Improved Pressure Resistance and Low Structural Parameter

Keizo Nakagawa[1]*, Kiyohito Uchida[1], Jiang Ling Chuan Wu[1], Takuji Shintani[1], Tomohisa Yoshioka[1], Yuji Sasaki[2], Li-Feng Fang[3], Eiji Kamio[2], Ho Kyong Shon[4], and Hideto Matsuyama[1,2]*

[1]Research Center for Membrane and Film Technology, Graduate School of Science, Technology and Innovation, Kobe University, 1-1 Rokkodai, Nada, Kobe 657-8501, Japan.

[2]Research Center for Membrane and Film Technology, Department of Chemical Science and Engineering, Kobe University, 1-1 Rokkodai, Nada, Kobe 657-8501, Japan.

[3]Engineering Research Center of Membrane and Water Treatment (Ministry of Education), Department of Polymer Science and Engineering, Zhejiang University, Hangzhou 310027, China.

[4]Centre for Technology in Water and Wastewater, School of Civil and Environmental Engineering, University of Technology Sydney (UTS), PO Box 123, 15 Broadway, Ultimo, NSW 2007, Australia.

*Corresponding Authors:

E-mail addresses: k.nakagawa@port.kobe-u.ac.jp (K. Nakagawa), matuyama@kobe-u.ac.jp (H. Matsuyama)

Abstract

In this study, we fabricated porous polyketone (PK) support membranes with high pressure resistance and low structural parameter (*S*) by surface modification with aromatic compounds for osmotically driven membrane process applications. The effects of surface modification of PK using aromatic compounds on the membrane structure, mechanical properties, and membrane performance were investigated. Based on an estimation of the affinity between PK and aromatic compounds using Hansen solubility parameters and mechanical properties, *m*-phenylenediamine (MPD) was selected as an appropriate chemical modifier for PK membranes. The PK support membranes modified with MPD (PK-MPD) had a dense structure on the bottom side. The thickness and porosity of the PK membranes were changed by the treatment temperature. As a result, polyamide (PA)/PK-MPD thin film composite membranes showed superior pressure resistance in reverse osmosis. PA/PK-MPD modified at 110 °C possessed the highest pressure resistance of 21 bar, which was 3.5 times higher than that of the PA/untreated PK membrane, while maintaining a high water flux of 19.4 L m^{-2} h^{-1} in FO. This performance overcame the trade-off relationships between pressure resistance and FO flux and between pressure resistance and *S* value.

Keywords: polyketone, porous membrane, surface modification, pressure resistance, structural parameter, forward osmosis

1. Introduction

Osmotically driven membrane processes have received much attention because of their great potential for various applications such as desalination and water treatment [1,2] and solution concentration [3–5] by forward osmosis (FO) and energy production by pressure retarded osmosis (PRO)[6]. In FO process, the semipermeable FO membrane is set between a draw solution (DS) with high osmotic pressure and a feed solution (FS) with low osmotic pressure. The DS draws water from the FS through the FO membrane by osmotic pressure difference, therefore, hydraulic pressure is basically not necessary for water permeation. Toward an industrial application utilizing the FO membrane process, the development of new DS materials and efficient regeneration systems to separate water from the diluted DS is required. Furthermore, the development of a highly water-permeable FO membranes is also important. Thin-film composite (TFC) membranes, which are composed of a selective active layer and a porous support layer, are often used as FO membranes. Especially, as the support layer, a very thin and highly porous structure with low tortuosity, namely low structural parameter (S), is preferred to suppress the effect of internal concentration polarization (ICP) on membrane performance [7,8].

On the other hand, the development of FO membranes with high water flux and pressure resistance has been recently required because the FO membranes can be utilized in the osmotically driven membrane processes which are operated under hydraulic pressurized condition such as PRO [6] and pressure-assisted forward osmosis (PAO) [9]. Wan et al. reported that highest power density

was obtained at around 20 bar in PRO process using seawater brine as DS and deionized water as FS [6]. Oh et al. reported that water flux was improved with increasing the applied hydraulic pressure (3.9 - 20.7 bar) in FO mode (active layer facing to feed solution) in PAO process [9]. Thus the FO membranes for PRO and PAO processes must possess good pressure resistance. The design of support membranes with low structural parameter and high pressure resistance is topical and desirable.

Various porous support membranes have been reported, such as polysulfone (PSf) [10,11], polyethersulfone (PES) [12,13], sulfonated polyethersulfone (SPES) [14,15], cellulose acetate [16,17], polyvinylidene fluoride (PVDF) [18,19], and polyacrylonitrile (PAN) [20,21]. Recently, our research group has focused on an aliphatic polyketone (PK) support for the development of TFC membranes [22–28]. The PK support membranes, which are prepared by nonsolvent-induced phase separation (NIPS), have a sponge-like porous structure. Interfacial polymerization has further been performed to form a polyamide (PA) selective layer on the PK membrane (PA/PK). Owing to their hydrophilic nature, highly porous structure, and organic solvent resistance, PA/PK membranes have been used in various applications, such as oil–water separation [22,23], as an enzyme membrane reactor (EMR) in organic solvent [24], and in FO processes [25–28]. In particular, FO membranes using a PK support membrane have shown relatively high water flux compared with other reported FO membranes prepared using different types of support membrane. However, the pressure resistance of the PA/PK membranes is not enough because of the highly porous structure of PK support [25]. Several approaches have been reported to improve the pressure resistance of FO membranes, for example, thickening the support

membrane [27] and introducing nonwoven fabric materials into the FO membrane [28,29]. However, such approaches induce an increase in the ICP owing to the increase of the support thickness, resulting in lower water flux. In this situation, the morphology control of the support membrane is alternative to satisfy the requirement of the pressure resistance and low structural parameter.

In this study, we focused on the solubility characteristic of PK to control the morphology of PK support membrane. In the PK membrane preparation by NIPS method, an aromatic compound such as resorcinol is used as a solvent [25]. Therefore, we performed surface modification of the PK membrane with various aromatic compounds based on an estimation of the affinity between PK and aromatic compounds using Hansen solubility parameters (HSPs). The effects of surface modification on the membrane structure, mechanical properties, and FO membrane performance were investigated in detail.

2. Experimental

2.1. Chemicals

Aliphatic PK powder (Mw: 700,000; Asahi Kasei, Tokyo, Japan) was used as a support material. Resorcinol, methanol, acetone, and hexane (Fujifilm Wako Pure Chemical, Osaka, Japan) were used to prepare the PK support membrane. Aniline, *m*-phenylenediamine (MPD), and *m*-cresol (Tokyo Chemical Industry, Tokyo. Japan) were used for surface modification of the PK support membrane. MPD, 1,3,5-benzenetricarbonyl trichloride (TMC), 10-camphorsulfonic acid (CSA) (Tokyo Chemical Industry), sodium dodecyl sulfate (SDS), and triethylamine (TEA) (Fujifilm Wako Pure Chemical)

were used to prepare PA active layer. Sodium chloride (Fujifilm Wako Pure Chemical) aqueous solution was used for the RO and FO measurements. Ultrapure water was produced by a Milli-Q ultrapure water system (Merck Millipore, Billerica, MA, USA) and used to prepare FS and DS solutions.

2.2. Preparation of porous PK support membrane

The preparation of flat-sheet porous PK membranes was performed by NIPS according to a previous report [25]. A mixture of PK powder, resorcinol, and water (mass ratio, 10.0:58.5:31.5) was stirred at 80 °C for 3 h and then kept at 50 °C in an oven overnight to remove gas bubbles. The polymer solution was cast onto a glass plate (casting height, 200 μm) using an applicator (Yoshimitsu Seiki YBA-4 type, Irie Shokai, Tokyo, Japan). The cast membrane on the glass plate was immersed in a coagulation bath of methanol/water (mass ratio, 30:70) for 20 min. The PK membrane was then washed alternately with acetone and hexane for 20 min to remove residual resorcinol and water.

2.3. Modification of PK support membranes with aromatic compounds

In the preparation of the PK membrane by NIPS, resorcinol is used as a solvent. Therefore, some aromatic compounds with different functional groups and physical properties were selected as candidates for the modification of PK, namely *m*-cresol, aniline, resorcinol, and MPD, as shown in Fig. 1. The PK membranes were modified with each aromatic compound at different temperatures.

The concentration of the aromatic compound in aqueous solution was controlled at 2.0 or 5.0 wt%. The PK membranes were clipped with a pair of Teflon frames and the aromatic compound aqueous solution was poured onto the top side of the as-prepared PK membrane. After 2 min, the solution was removed and the bottom side of the PK membrane was modified in the same way as the top side. The modified PK membranes were then heat-treated in an oven at different temperatures (50, 70, 90, 110, and 130 °C) for 10 min. After cooling at room temperature for 30 min, the PK membranes were washed with acetone for 20 min to remove residual aromatic compound and water. The modified PK support membranes were denoted using the abbreviated name of the aromatic compound and the treatment temperature; for example, PK-Cre-90, PK-Ani-90, PK-Res-90, and PK-MPD-90.

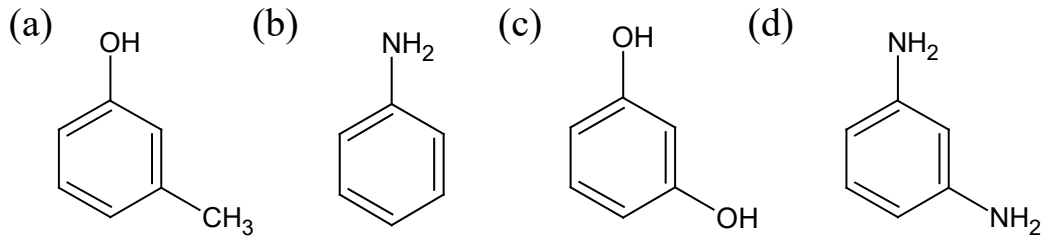

Fig. 1. Chemical structures of aromatic compounds (a) *m*-cresol, (b) aniline, (c) resorcinol, and (d) *m*-phenylenediamine.

HSPs [30] were used to quantify the affinity between different chemical species. HSPs are characterized by three force factors, namely, dispersion, dipole interaction, and hydrogen bonding, according to equation (1):

$$\delta_{\mathrm{t}} = \left(\delta_d^2 + \delta_p^2 + \delta_h^2\right)^{1/2}, \quad (1)$$

where δ_{d}, δ_{p}, and δ_{h} ($\mathrm{MPa}^{1/2}$) are the solubility contributions from the dispersion force factor, the

dipole interaction force factor, and the hydrogen-bonding force factor, respectively, and δ_t ($MPa^{1/2}$) is the total HSP. The HSPs of PK, aromatic compounds, and water are listed in Table 1. The affinity between two substances can be determined from the difference in the HSP values (R_a), as expressed by equation (2):

$$R_a = \left(4(\delta_{d1} - \delta_{d2})^2 + \left(\delta_{p1} - \delta_{p2}\right)^2 + (\delta_{h1} - \delta_{h2})^2\right)^{1/2}, \quad (2)$$

where a smaller R_a value indicates a higher affinity.

Table 1. Hansen solubility parameters of polyketone (PK), aromatic compounds, and water, and the estimated distance between PK and aromatic compounds or water (R_a).

Substance	δ_d [$MPa^{1/2}$]	δ_p [$MPa^{1/2}$]	δ_h [$MPa^{1/2}$]	δ_t [$MPa^{1/2}$]	R_a [$MPa^{1/2}$]
PK	19.2	17.9	6.8	27.1	-
m-Cresol	18.3	4.9	13.9	23.5	14.8
Aniline	18.8	1.2	9.6	21.2	16.9
Resorcinol	19.5	8.3	21.5	30.2	17.5
MPD	19.3	1.2	13.3	23.4	17.9
Water	15.5	16.0	42.3	47.8	35.7

2.4. Preparation of polyamide (PA) active layer

A PA active layer was prepared on the top side of the PK membranes by interfacial polymerization according to a previous report [5,25]. An aqueous solution containing SDS (0.25 wt%), MPD (2.0 wt%), TEA (2.0 wt%), and CSA (4.0 wt%), and a hexane solution containing TMC (0.15 wt%) were prepared. The PK membrane was immersed in the aqueous solution for 1 min. After removing the aqueous solution, the hexane solution was poured onto the PK membrane and left for 30 s to form a

PA layer through interfacial polymerization. After removing the hexane solution, the PK membrane was treated at 100 °C for 5 min. Then as-prepared membranes were washed with Milli-Q water. The as-obtained PA TFC membranes were denoted using the names of the prepared PK support membrane; for example, PA/PK-MPD-90.

2.5. Membrane characterization

Mechanical properties, such as the fracture stress, fracture strain, and Young's modulus of the PK support membranes, were measured using a tensile tester (EZ-LX, Shimadzu, Kyoto, Japan) [31]. For the stretching test, a membrane (35×4 mm) was attached to the instrument with 50 mm between the jigs. A uniaxial stretching test was conducted by stretching the membrane at a constant strain rate of 30 mm min^{-1}. The thickness of the as-prepared PK membranes was measured using a dial thickness gauge (Ozaki Mfg, Tokyo, Japan). The bulk porosity of the PK membrane was estimated using equation (3):

$$\text{Porosity } [\%] = \left(1 - \frac{W}{A\rho t \times 10^{-4}}\right), \quad (3)$$

where W (g) is the mass of the PK membrane, A (cm^2) is the PK membrane area, ρ is the density of PK (1.30 g cm^{-3}), and t (μm) is the membrane thickness of PK measured using a dial thickness gauge. The porous structure of the prepared PK membranes was observed by field-emission scanning electron microscopy (FE-SEM; JSM-7500F, JEOL, Tokyo, Japan). The surface chemical properties of the prepared PK membranes were measured by X-ray photoelectron spectroscopy (XPS; JPS-9200, JEOL)

and attenuated total reflection–Fourier transform infrared spectroscopy (ATR-FTIR; Thermo Fisher Scientific, Waltham, MA, USA).

2.6. RO and FO measurements

A cross-flow RO membrane filtration system was used to evaluate water permeability, salt rejection, and salt permeability according to a previous report [5]. The effective membrane area was 8.04 cm^2. Milli-Q water and NaCl aqueous solution (2000 ppm) were supplied at a flow rate of 9.9 mL min^{-1} and the permeate solution was measured for 30 min, after which an additional pressure of 1 bar was applied. The water permeability coefficient A (L m^{-2} h^{-1} bar^{-1}] was estimated from equation (4):

$$A = \frac{J_{\mathrm{W(water)}}^{\mathrm{RO}}}{\Delta P}, \tag{4}$$

where $J_{\mathrm{W(water)}}^{\mathrm{RO}}$ (L m^{-2} h^{-1}) is pure water flux when using Milli-Q water as the feed solution and ΔP (bar) is the transmembrane pressure difference. The salt permeability coefficient B (L m^{-2} h^{-1}) was estimated from the apparent salt rejection R_{app} (no unit) and mass transfer coefficient $k_{\mathrm{f}}^{\mathrm{RO}}$ (L m^{-2} h^{-1}), obtained using equations (5)–(7) [32]:

$$B = J_{\mathrm{W(NaCl)}}^{\mathrm{RO}} \left(\frac{1-R_{app}}{R_{\mathrm{app}}}\right) \exp\left(-\frac{J_{\mathrm{W(NaCl)}}^{\mathrm{RO}}}{k_{\mathrm{f}}^{\mathrm{RO}}}\right), \tag{5}$$

$$R_{\mathrm{app}} = 1 - \frac{C_{\mathrm{p}}}{C_{\mathrm{f}}}, \tag{6}$$

$$k_{\mathrm{f}}^{\mathrm{RO}} = \frac{J_{\mathrm{W(NaCl)}}^{\mathrm{RO}}}{\ln\left(\frac{\Delta P}{\pi_{\mathrm{f}}-\pi_p}\left(1-\frac{J_{\mathrm{W(NaCl)}}^{\mathrm{RO}}}{J_{\mathrm{W(water)}}^{\mathrm{RO}}}\right)\right)}, \tag{7}$$

where C_{p} and C_{f} (mol L^{-1}) are the salt concentrations of the permeate solution and feed solution,

respectively, $J_{W(NaCl)}^{RO}$ is the water flux when using 2000 ppm NaCl solution as the feed solution, and π_f and π_p are the osmotic pressures of the bulk feed solution and permeate solution, respectively.

The pressure resistance of the PA/PK membranes was evaluated by successive control of the transmembrane pressure difference using the same cross-flow RO membrane filtration system according to a previous report [27]. The critical pressure $P_{Critical}$ (bar) was determined from the drastic increase in water flux and decrease in apparent rejection while increasing the transmembrane pressure difference, which implied breakage of the membrane under that pressure.

To determine the FO performance, the water flux J_W^{FO} (L m^{-2} h^{-1}) and reverse salt diffusion J_S^{FO} (g m^{-2} h^{-1}) of the PA/PK membranes were measured using a cross-flow FO membrane filtration system according to a previous report [5]. The effective membrane area was 4.5 cm^2. Both FS (Milli-Q water, 700 mL) and DS (NaCl aqueous solution from 0.3 to 1.0 M, 800 mL) were continuously supplied at a flow rate of 500 mL min^{-1} with a counter flow pattern for 1 h. J_W^{FO} and J_S^{FO} were calculated by recording the volume reduction and the increase in the solute amount in the FS, respectively. Mesh spacers were attached to the DS and FS sides to improve the turbulence of the feed flows and prevent the effect of external concentration polarization on membrane performance. The osmotic pressure of the DS was measured using a freezing point osmometer (Osmomat 3000 basic, Gonotec, Berlin, Germany). FO measurements were conducted in FO mode (active layer facing to feed solution, AL-FS). The structural parameter S (μm), which is defined as the diffusion resistance of DS in the support layer, is a key parameter in FO performance. S is determined by the thickness (t, μm), porosity (ε), and

tortuosity (τ) according to equation (8) [33]:

$$S = \frac{\tau t}{\varepsilon}. \quad (8)$$

The S values of the prepared membranes were fitted with the A, B, and water flux ($J_{\mathrm{W}}^{\mathrm{FO}}$) values obtained from experiments using different DS concentrations by equations (9) [34]:

$$J_{\mathrm{W}}^{\mathrm{FO}} = \frac{D}{S}\ln\left(\frac{B + A\pi_{DS}}{B + A\pi_{\mathrm{FS}} + J_{\mathrm{W}}^{\mathrm{FO}}}\right) \quad (9)$$

where D (m^2 s^{-1}) is the bulk diffusivity of the DS, and π_{DS} and π_{FS} (bar) are the osmotic pressures of DS and FS, respectively.

3. Results and discussion

3.1 Fabrication and characterization of PK support membranes modified with aromatic compounds

The R_a values between PK and aromatic compounds or water were estimated using HSP values, as shown in Table 1. The R_a values of the aromatic compounds are apparently smaller than that of water, indicating that these aromatic compounds have a better affinity for PK than water. The R_a value of *m*-cresol is the lowest among the aromatic compounds, while those of aniline, resorcinol, and MPD are estimated to be around 17–18. Based on this estimation of the affinity for PK, both surfaces of the PK support membranes prepared using the NIPS method were modified with aromatic compounds. Structural analysis of the modified PK membranes was performed using a tensile tester, FE-SEM, XPS, and ATR-FTIR.

Table 2 shows the mechanical properties (maximum tensile strength, elongation at break, and

Young's modulus) of the modified PK membranes. For comparison, PK membranes were treated in water without an aromatic compound or dried in air at 90 °C for 10 min (denoted as PK-Water-90 and PK-Air-90, respectively), with the results for these membranes also listed in Table 2. For PK-Water-90, the elongation at break is lower compared with that of pristine PK membrane (PK (Untreated)). This result indicates that the PK membrane becomes brittle with heat treatment in water. However, the PK membranes modified with aromatic compounds show different behavior. The aromatic compound concentration was controlled at 2.0 wt% owing to the limited solubility of *m*-cresol in water. For *m*-cresol, which has the lowest R_a value, the PK membrane was partially dissolved in *m*-cresol aqueous solution, as observed by the naked eye, and no mechanical property data were obtained. Although aniline has a smaller effect on the mechanical properties of PK, the surface modification of PK with resorcinol and MPD significantly affects the tensile strength, which changes from 3.7 MPa (PK (Untreated)) to 10.5 MPa (PK-Res-90) and 7.3 MPa (PK-MPD-90). The surface modification of PK with MPD affords high elongation at break values. Notably, the color of some parts of the PK membrane modified with resorcinol changed from white to transparent, implying large pores changing into small pores or loss of the porous structure. Therefore, among the aromatic compounds, MPD was selected as an appropriate chemical modifier.

The effect of treatment temperature during surface modification of PK with MPD (5.0 wt%) on the mechanical properties was studied further (Table 2, Fig. 2). The maximum tensile strength values clearly increase with increasing treatment temperature. The color of some parts of the PK membrane

modified with MPD (5 wt%) at 130 °C also changed from white to transparent, and no data were obtained. The change of the porous structure will be discussed later. The maximum tensile strength of PK-MPD-90 (5.0 wt%) is higher than that of PK-MPD-90 (2.0 wt%). Therefore, surface modification of PK with MPD is confirmed to enhance the mechanical properties of PK membranes. The values of the maximum tensile strength of PK-MPD-90 (5.0 wt%) and PK-MPD-110 (5.0 wt%) are found to be similar to or higher than those of the reported PES, PES-SPES and PVDF FO membranes [13,15,19], implying that the PK membranes modified with MPD have suitable mechanical properties for the application of osmotically driven membrane processes.

Table 2. Mechanical properties of the PK and modified PK support membranes with those of the reported support and TFC membranes for FO. (*NA: not available)

Membrane	Concentration of aromatic compound [wt%]	Maximum tensile strength [MPa]	Elongation at break [%]	Young's modulus [MPa]
PK (Untreated)	-	3.7±0.3	19.8±3.3	45.9±2.2
PK-Cre-90	2.0	NA*	NA	NA
PK-Ani-90	2.0	3.7±0.4	23.4±1.8	75.6±5.2
PK-Res-90	2.0	10.5±1.2	16.5±0.6	204.7±5.2
PK-MPD-90	2.0	7.3±0.6	32.2±0.8	155.7±4.3
PK-MPD-50	5.0	4.5±0.5	25.2±1.5	98.0±5.3
PK-MPD-70	5.0	5.6±0.6	22.7±6.2	148.7±4.3
PK-MPD-90	5.0	7.9±0.4	25.8±5.2	177.0±5.8
PK-MPD-110	5.0	10.4±0.8	24.9±5.4	284.7±14.1
PK-Water-90	-	3.8±0.4	18.0±1.5	79.7±8.8
PK-Air-90	-	2.7±0.7	20.1±2.6	48.8±3.6
[a]PES [13]	-	6.97±0.23	49.82±8.34	228.30±49.56
[b]PES [15]	-	7.8	17.9	241
[b]PES-SPES [15]	-	1.1	43.3	12
[c]PVDF [19]	-	6.92±0.59	143.04±23.59	31.94±9.17

[a] Hollow fiber membrane, [b] Polyamide-based TFC membrane, [c] Electrospun nanofiber membrane

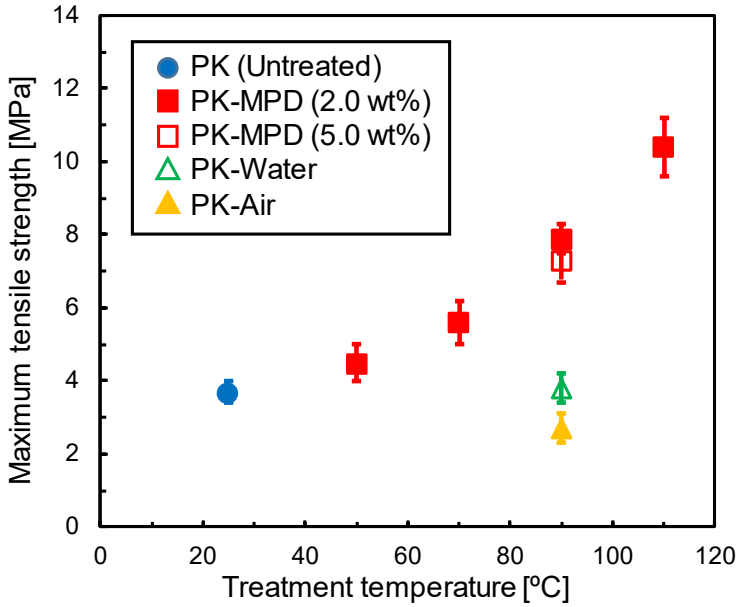

Fig. 2. Effect of treatment temperature on the maximum tensile strength of the modified PK membranes with MPD.

To determine the effect of MPD treatment of PK membranes on the membrane structure, the top side, bottom side, and cross-section of the PK membranes, and those modified with MPD (Figs. 3 and 4), were observed by FE-SEM. The PK (Untreated) membrane has an asymmetric structure. A fibril structure is observed on the bottom side, while a dense structure is observed on the top side (Figs. 3a and 3d). FE-SEM images of the cross-section show that PK (Untreated) has sponge-like pores of around 2–3 μm. Small pores of less than 1 μm are also observed near the top-side surface. PK membranes with similar porous structures have been reported in the previous study [25]. The membrane thickness is around 70 μm. The PK-Air-90 and PK-Water-90 membranes have porous structures that are similar to that of the PK (Untreated) membrane.

In contrast, PK membranes modified with MPD show unique morphological changes. The fibril structures on the bottom side are denser for PK-MPD-90 and PK-MPD-110 (Figs. 4g and 4h) and the

porous structures on the top side are slightly denser (Figs. 4c and 4d). Furthermore, PK membranes modified with MPD become thinner (down to 40–50 μm; Figs. 4k and 4l) than the PK (Untreated) membrane. Fig. S1 (see supplementary information) also shows the SEM images of the top side, bottom side, and cross-section of the PK-MPD-130 membrane. Less porous structure is observed on the top side, and much denser fibril structure is formed while maintaining the porous structure on the bottom side. The ATR-FTIR and XPS measurements shown in Fig. S2 and Table S1 indicate little difference in chemical structure between the untreated and MPD-modified membranes. Compared with the PK (Untreated) membrane, the membrane thickness of PK membranes modified with MPD largely decreases while that of PK-Water-90 slightly decreases. During the surface modification with MPD, the structures on both sides are assumed to be partially melted in the MPD aqueous solution at relatively high temperatures (90, 110 and 130 °C). At the same time, the membrane thickness decreases due to the shrinkage upon heat treatment because of the strong interaction between PK and MPD. These factors would result in the formation of a dense structure mainly on the bottom side owing to the more porous original structure on the bottom side.

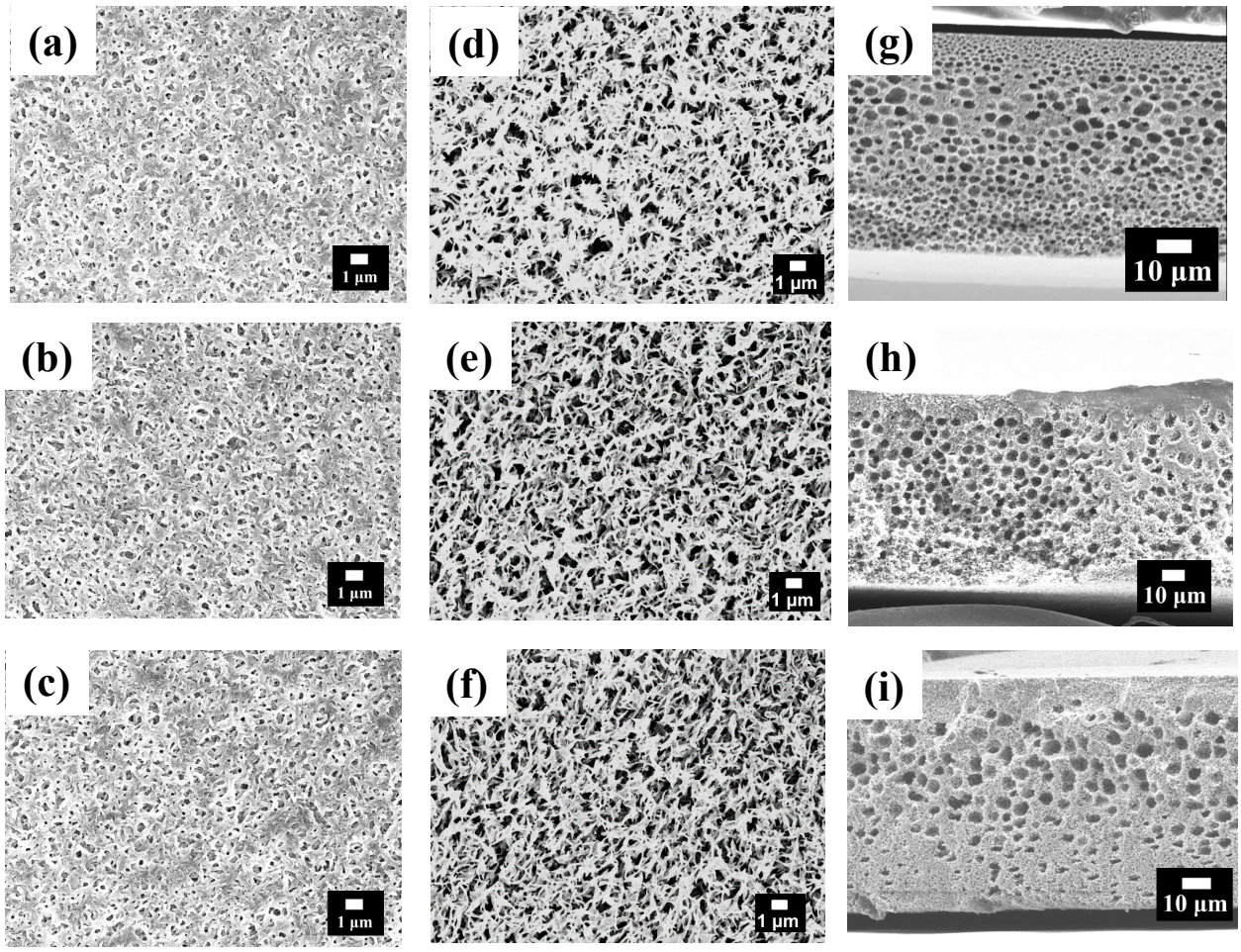

Fig. 3. SEM images of (a–c) top side, (d–f) bottom side, and (g–i) cross-section of (a,d,g) PK (Untreated), (b,e,h) PK-Air-90, and (c,f,i) PK-Water-90 membranes.

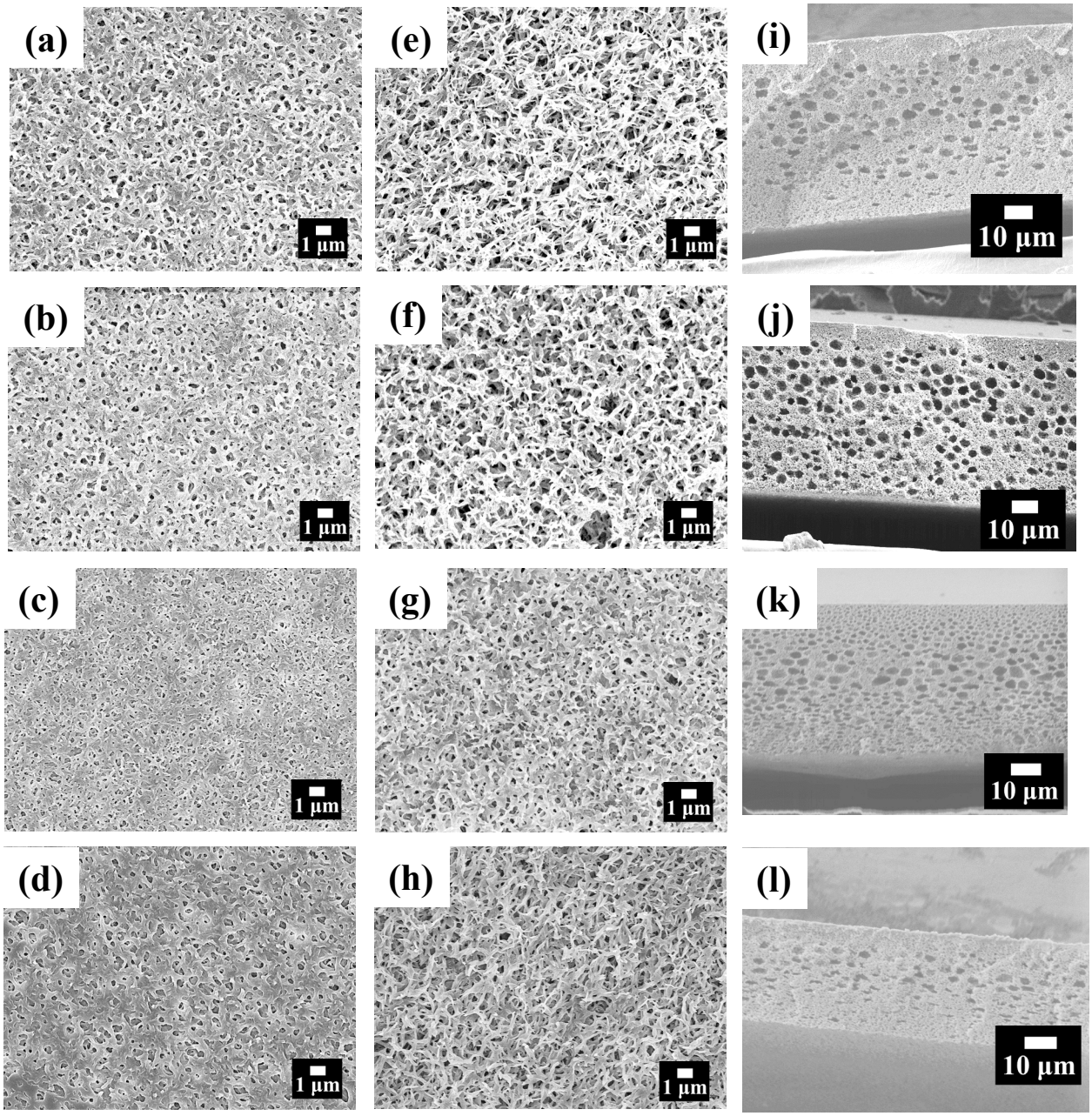

Fig. 4. SEM images of (a–d) top side, (e–h) bottom side, and (i–l) cross-section of (a,e,i) PK-MPD-50, (b,f,j) PK-MPD-70, (c,g,k) PK-MPD-90, and (d,h,l) PK-MPD-110 membranes.

Figure 5 shows the thickness ratio (modified PK membrane/PK membrane (Untreated)) and porosity of the PK membranes modified with MPD at different treatment temperatures. The membrane thickness was specifically measured using a dial thickness gauge to avoid structural changes during

FE-SEM measurement. Compared with the PK (Untreated) membrane, the membrane thickness of PK-Air-90 hardly changes, while that of PK-Water-90 slightly decreases to 90%. The PK membranes modified with MPD become thinner with increasing treatment temperature. These results are consistent with the SEM observations. Although the porosity decreases gradually with increasing treatment temperature, the porosity of all PK membranes remains at around 70%–80% owing to the dense structure being formed only on the near surface of the bottom side.

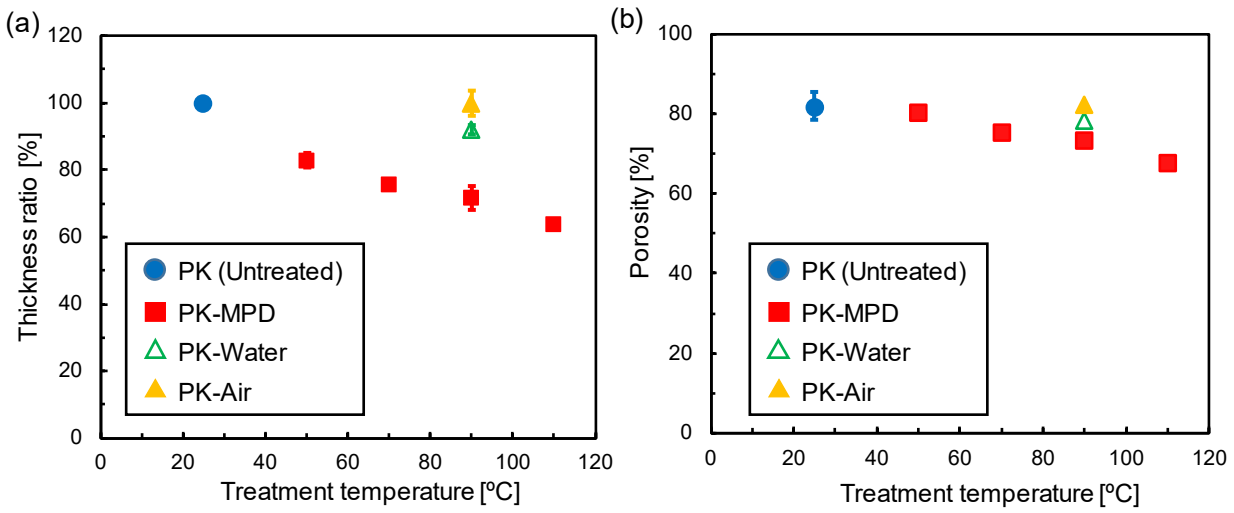

Fig. 5. Effect of treatment temperature on (a) thickness and (b) porosity of prepared PK support membranes.

3.2. RO and FO performances of PA/PK membranes

A PA active layer was prepared on the PK support membranes modified with MPD through interfacial polymerization. The RO performances of the PA/PK membranes modified with MPD are listed in Table 3. For all PA/PK membranes, the NaCl rejection is over 95% and the A values are 1.78–2.04 L m^{-2} h^{-1} bar^{-1}. These A values are lower than those reported for PA/PK membranes and

PA/polyethersulfone (PES)-sulfonated polyethersulfone (SPES) membranes, but higher than those of commercially available cellulose triacetate (CTA) and PA/PES membranes. The formation of a PA active layer has been reported to be affected by the pore size and surface properties of the top side of the support, which affects the RO performance [35]. The porous structures on the top side of the PK membranes modified with MPD are slightly denser than that of the PK (Untreated) membrane (Figs. 3 and 4), however, little difference in the RO performance is observed among the PA/PK membranes because of the small change of the porous structures on the top side.

The FO performances of the PA/PK membranes modified with MPD were measured in FO mode using different DS concentrations (Table 3, Fig. 6). The FO flux increases with increasing DS concentration owing to the increased driving force (osmotic pressure difference) (Fig. 6a). The PA/PK membranes modified with MPD at several temperatures show similar J_W^{FO} values of 17.2–19.4 L m^{-2} h^{-1}. These values are higher than those of the commercial CTA membrane, but slightly lower than those of previously reported PA/PK membranes. Fig. 6b shows the results of specific reverse salt flux (J_S^{FO}/J_W^{FO}) of various PA/PK membranes. The values of J_S^{FO}/J_W^{FO} of the PA/PK membranes are lower than that of the commercial CTA membrane, suggesting the formation of PA/PK FO membranes with better selectivity. Theoretical fitting curves shown as solid lines in Fig. 6 were obtained from equation (9) using *A* and *B* values. The *S* values obtained from the fitting are also listed. The *S* values are found to be lower than those of the commercial CTA membrane and reported PA/PK membranes.

Table 3. Comparison of RO and FO performances of PA/PK membranes modified with MPD with those of the reported membranes and commercial membranes. All experimental conditions are identical.

Membrane	A [LMH/bar]	B [LMH]	Rejection [%]	$P_{Critical}$ [bar]	C_{DS} [mol/L]	J_W^{FO} [LMH]	J_S^{FO} [gMH]	S [μm]	Ref.
PA/PK (Untreated)	2.04 ±0.09	0.304 ±0.107	96.1 ±0.7	6	0.5	18.7 ±2.2	2.57 ±0.56	249 ±11	This work
PA/PK-MPD-50	1.78 ±0.22	0.227 ±0.122	95.8 ±2.3	8	0.5	17.7 ±0.4	2.37 ±0.43	272 ±34	This work
PA/PK-MPD-70	1.91 ±0.28	0.341 ±0.081	95.8 ±2.6	13	0.5	19.0 ±2.1	2.02 ±0.29	254 ±35	This work
PA/PK-MPD-90	1.83 ±0.12	0.207 ±0.055	95.7 ±0.3	15	0.5	17.2 ±2.0	2.25 ±0.61	246 ±16	This work
PA/PK-MPD-110	1.78 ±0.15	0.228 ±0.108	96.1 ±1.4	21	0.5	19.4 ±1.9	2.71 ±0.35	263 ±20	This work
CTA (FTS)	0.695	0.043	98.2	>40	0.5	7.03	2.42	636	This work
PA/PK (PA-1)	1.21	0.20	-	12	0.6	13.8	2.75	364	[25]
PA/PK (PA-2)	1.84	0.21	-	11	0.6	19.7	3.45	287	[25]
PA/PK (PA-3)	2.50	0.18	-	10	0.6	24.4	3.33	280	[25]
PA/PK (PK-1)	2.42	0.370	-	6	0.6	22.1	3.62	261	[27]
PA/PK (PK-2)	2.65	0.310	-	6	0.6	27.9	3.74	205	[27]
PA/PK (PK-3)	2.79	0.54	-	4	0.6	30.3	4.56	176	[27]
PA/PK (PK-4)	-	-	-	2	0.6	31.3	8.94	-	[27]
PA/PES	1.18	0.135	88.0	-	0.5	22.5	2.80	219	[13]
PA/PES-SPES	2.90	0.184	91.1	-	0.5	17.6	7.05	245	[15]

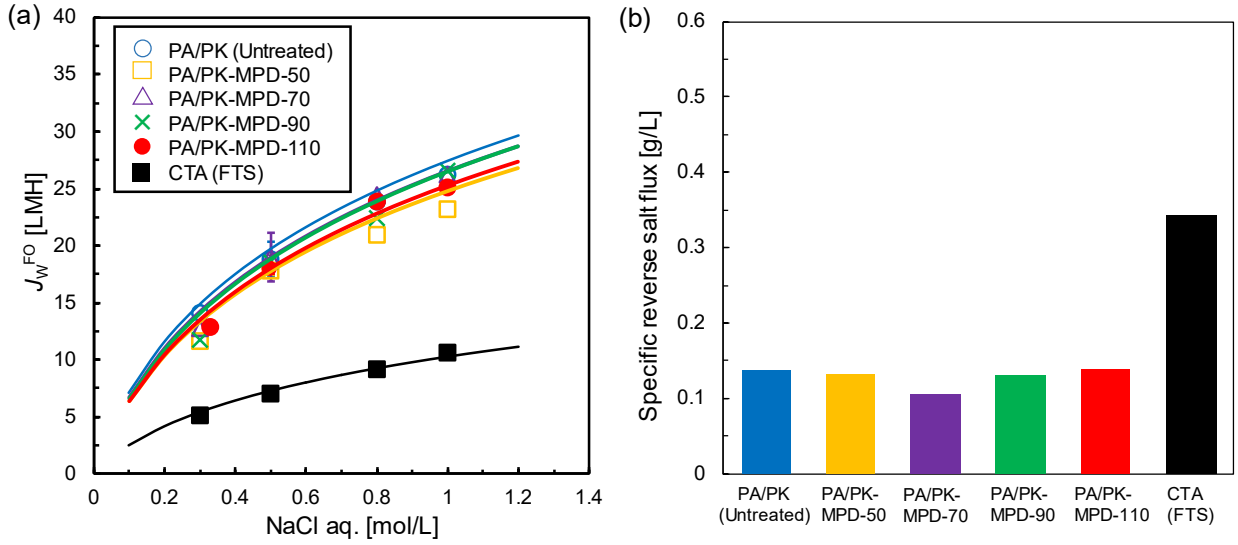

Fig. 6. (a) Water flux results for PA/PK membranes at different NaCl concentrations and (b) specific reverse salt flux (J_S^{FO}/J_W^{FO}) of various PA/PK membranes with the commercial CTA membrane.

Table 3 also shows the pressure resistance of the PA/PK membranes, as evaluated by successively increasing the transmembrane pressure difference using cross-flow RO membrane filtration. The PA/PK (Untreated) membrane shows a $P_{Critical}$ value of 6 bar, which is similar to or slightly lower than those of reported PA/PK membranes. Interestingly, the $P_{Critical}$ values of PA/PK membranes modified with MPD are higher than that of the PA/PK (Untreated) membrane, with the values drastically increasing with increasing treatment temperature. Notably, the PA/PK-MPD-110 membrane shows the highest $P_{Critical}$ value of 21 bar, which is 3.5 times higher than that of PA/PK (Untreated). These results appear to show the same tendency as the mechanical properties results (Fig. 2). Therefore, the tensile strength of the PK membranes is considered to be directly affected by the pressure resistance, as estimated by RO measurements.

Figure 7 shows the relationships between P_{Critical} and FO flux ($J_{\mathrm{W}}^{\mathrm{FO}}$) values and between P_{Critical} and *S* values for the PA/PK membranes modified with MPD and previously reported PA/PK membranes. Some data for previously reported PA/PK membranes (black squares) showed high $J_{\mathrm{W}}^{\mathrm{FO}}$ values of over 20 L m^{-2} h^{-1} (Fig. 7a) or low *S* values of around 200 μm (Fig. 7b), but with relatively low P_{Critical} values of less than 13 bar. The trade-offs between P_{Critical} and $J_{\mathrm{W}}^{\mathrm{FO}}$ and between P_{Critical} and *S* values are clearly shown by dotted lines. The results for PA/PK (Untreated) and PA/PK-MPD-50 are located along the trade-off relationship. Notably, the PA/PK-MPD-70, 90, and 110 membranes overcome these trade-off relationships. These important results have not been reported previously. The PA/PK membranes modified with MPD achieve superior pressure resistance while maintaining high $J_{\mathrm{W}}^{\mathrm{FO}}$ values owing to the low *S* values (Table 3). Using equation (8), the *S* values were determined from the thickness, porosity, and tortuosity. Although modifying PK with MPD decreases the porosity of the PK membranes, the magnitude of this decrease is marginal (Fig. 5b). However, the membrane thickness is significantly decreased by surface modification (Fig. 5a). Therefore, we assume that such a decrease in membrane thickness is correlated with low *S* values, leading to the high FO water flux. Further improvements in the membrane structure of PK membranes would be expected by optimizing the porous structure and membrane thickness of the original PK membranes using modification agents.

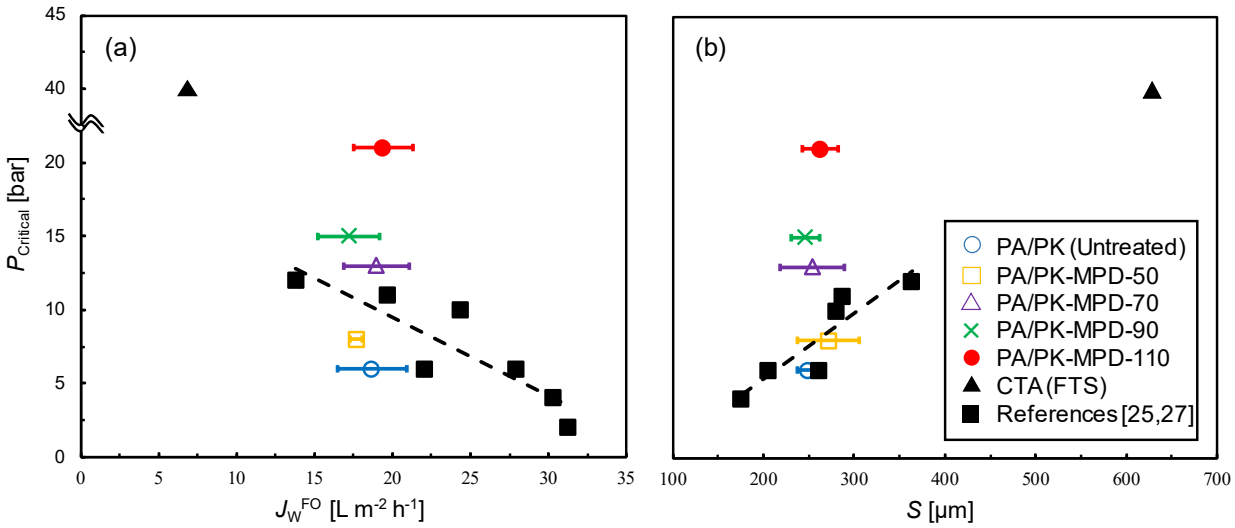

Fig. 7. Relationship between pressure resistance (P_{Critical}) and (a) FO flux ($J_{\mathrm{W}}^{\mathrm{FO}}$) and (b) S value for the PA/PK membranes modified with MPD and reported PA/PK membranes.

4. Conclusions

PK membranes were modified with aromatic compounds to improve the mechanical properties and membrane performance. MPD was selected as an appropriate chemical modifier for PK membranes by considering the affinity between PK and MPD based on HSP and the results of mechanical property testing. PK fibril structures on the bottom side became more dense for PK membranes through surface modification with MPD. As a result, PK membranes modified with MPD showed superior pressure resistance. The pressure resistance of PA/PK-MPD membranes increased with increasing treatment temperature. Owing to the high porosity and reduced thickness, the PA/PK membranes modified with MPD showed low S values and high FO water flux. Therefore, these membranes were able to overcome the trade-off relationships between pressure resistance and FO flux and between pressure resistance

and *S* value. Owing to their superior characteristics, PK membranes might have applications not only in FO-related processes but also in RO-related processes such as osmotically-assisted reverse osmosis (OARO) whose water permeation is also affected by ICP in the support membrane [36,37] and organic solvent reverse osmosis (OSRO) [38]. Therefore, porous PK membranes with good mechanical properties are expected to show great potential in various practical applications.

Acknowledgments

This work was supported by the Japan Society for the Promotion of Science through Grants-in-Aid for Scientific Research (grant numbers 18H03854 and 19K05121), and partially supported by King Abdullah University of Science and Technology (KAUST) with the grant title of Competitive Research Grant 2017 (CRG 2017).

References

[1] T.Y. Cath, A.E. Childress, M. Elimelech, Forward osmosis: Principles, applications, and recent developments, J. Membr. Sci. 281 (2006) 70–87. https://doi.org/10.1016/j.memsci.2006.05.048.

[2] K. Lutchmiah, A.R.D. Verliefde, K. Roest, L.C. Rietveld, E.R. Cornelissen, Forward osmosis for application in wastewater treatment: A review, Water Res. 58 (2014) 179–197. https://doi.org/10.1016/j.watres.2014.03.045.

[3] Q. Yang, K.Y. Wang, T.S. Chung, A novel dual-layer forward osmosis membrane for protein enrichment and concentration, Sep. Purif. Technol. 69 (2009) 269–274. https://doi.org/10.1016/j.seppur.2009.08.002.

[4] X. Zhang, Z. Ning, D.K. Wang, J.C. Diniz da Costa, A novel ethanol dehydration process by forward osmosis, Chem. Eng. J. 232 (2013) 397–404. https://doi.org/10.1016/j.cej.2013.07.106.

[5] Y. Zhang, K. Nakagawa, M. Shibuya, K. Sasaki, T. Takahashi, T. Shintani, T. Yoshioka, E. Kamio, A. Kondo, H. Matsuyama, Improved permselectivity of forward osmosis membranes for efficient concentration of pretreated rice straw and bioethanol production, J. Membr. Sci. 566 (2018) 15–24. https://doi.org/10.1016/j.memsci.2018.08.046.

[6] C.F. Wan, T.S. Chung, Osmotic power generation by pressure retarded osmosis using seawater brine as the draw solution and wastewater retentate as the feed, J. Membr. Sci. 479 (2015) 148–158. https://doi.org/10.1016/j.memsci.2014.12.036.

[7] J.R. McCutcheon, M. Elimelech, Influence of concentrative and dilutive internal concentration polarization on flux behavior in forward osmosis, J. Membr. Sci. 284 (2006) 237–247. https://doi.org/10.1016/j.memsci.2006.07.049.

[8] S.S. Manickam, J.R. McCutcheon, Understanding mass transfer through asymmetric membranes during forward osmosis: A historical perspective and critical review on measuring structural parameter with semi-empirical models and characterization approaches, Desalination. 421 (2017) 110–126. https://doi.org/10.1016/j.desal.2016.12.016.

[9] Y. Oh, S. Lee, M. Elimelech, S. Lee, S. Hong, Effect of hydraulic pressure and membrane orientation on water flux and reverse solute flux in pressure assisted osmosis, J. Membr. Sci. 465 (2014) 159–166. https://doi.org/10.1016/j.memsci.2014.04.008.

[10] P. Xiao, L.D. Nghiem, Y. Yin, X.M. Li, M. Zhang, G. Chen, J. Song, T. He, A sacrificial-layer approach to fabricate polysulfone support for forward osmosis thin-film composite membranes with reduced internal concentration polarisation, J. Membr. Sci. 481 (2015) 106–114. https://doi.org/10.1016/j.memsci.2015.01.036.

[11] G. Han, S. Zhang, X. Li, N. Widjojo, T.S. Chung, Thin film composite forward osmosis membranes based on polydopamine modified polysulfone substrates with enhancements in both water flux and salt rejection, Chem. Eng. Sci. 80 (2012) 219–231.

https://doi.org/10.1016/j.ces.2012.05.033.
[12] L. Shi, S.R. Chou, R. Wang, W.X. Fang, C.Y. Tang, A.G. Fane, Effect of substrate structure on the performance of thin-film composite forward osmosis hollow fiber membranes, J. Membr. Sci. 382 (2011) 116–123. https://doi.org/10.1016/j.memsci.2011.07.045.
[13] P. Sukitpaneenit, T.S. Chung, High performance thin-film composite forward osmosis hollow fiber membranes with macrovoid-free and highly porous structure for sustainable water production, Environ. Sci. Technol. 46 (2012) 7358–7365. https://doi.org/10.1021/es301559z.
[14] N. Widjojo, T.S. Chung, M. Weber, C. Maletzko, V. Warzelhan, The role of sulphonated polymer and macrovoid-free structure in the support layer for thin-film composite (TFC) forward osmosis (FO) membranes, J. Membr. Sci. 383 (2011) 214–223. https://doi.org/10.1016/j.memsci.2011.08.041.
[15] S. Sahebi, S. Phuntsho, Y.C. Woo, M.J. Park, L.D. Tijing, S. Hong, H.K. Shon, Effect of sulphonated polyethersulfone substrate for thin film composite forward osmosis membrane, Desalination. 389 (2016) 129–136. https://doi.org/10.1016/j.desal.2015.11.028.
[16] M. Sairam, E. Sereewatthanawut, K. Li, A. Bismarck, A.G. Livingston, Method for the preparation of cellulose acetate flat sheet composite membranes for forward osmosis-Desalination using MgSO4 draw solution, Desalination. 273 (2011) 299–307. https://doi.org/10.1016/j.desal.2011.01.050.
[17] S. Zhang, K.Y. Wang, T.S. Chung, H. Chen, Y.C. Jean, G. Amy, Well-constructed cellulose acetate membranes for forward osmosis: Minimized internal concentration polarization with an ultra-thin selective layer, J. Membr. Sci. 360 (2010) 522–535. https://doi.org/10.1016/j.memsci.2010.05.056.
[18] M. Shibuya, M.J. Park, S. Lim, S. Phuntsho, H. Matsuyama, H.K. Shon, Novel CA/PVDF nanofiber supports strategically designed via coaxial electrospinning for high performance thin-film composite forward osmosis membranes for desalination, Desalination. 445 (2018) 63–74. https://doi.org/10.1016/j.desal.2018.07.025.
[19] M.J. Park, R.R. Gonzales, A. Abdel-Wahab, S. Phuntsho, H.K. Shon, Hydrophilic polyvinyl alcohol coating on hydrophobic electrospun nanofiber membrane for high performance thin film composite forward osmosis membrane, Desalination. 426 (2018) 50–59. https://doi.org/10.1016/j.desal.2017.10.042.
[20] J.Y. Lee, S. Qi, X. Liu, Y. Li, F. Huo, C.Y. Tang, Synthesis and characterization of silica gel-polyacrylonitrile mixed matrix forward osmosis membranes based on layer-by-layer assembly, Sep. Purif. Technol. 124 (2014) 207–216. https://doi.org/10.1016/j.seppur.2014.01.029.
[21] H.E. Kwon, S.J. Kwon, S.J. Park, M.G. Shin, S.H. Park, M.S. Park, H. Park, J.H. Lee, High performance polyacrylonitrile-supported forward osmosis membranes prepared via aromatic solvent-based interfacial polymerization, Sep. Purif. Technol. 212 (2019) 449–457. https://doi.org/10.1016/j.seppur.2018.11.053.
[22] L. Cheng, A.R. Shaikh, L.F. Fang, S. Jeon, C.J. Liu, L. Zhang, H.C. Wu, D.M. Wang, H.

Matsuyama, Fouling-Resistant and Self-Cleaning Aliphatic Polyketone Membrane for Sustainable Oil-Water Emulsion Separation, ACS Appl. Mater. Interfaces. 10 (2018) 44880–44889. https://doi.org/10.1021/acsami.8b17192.

[23] L. Zhang, L. Cheng, H. Wu, T. Yoshioka, H. Matsuyama, One-step fabrication of robust and anti-oil-fouling aliphatic polyketone composite membranes for sustainable and efficient filtration of oil-in-water emulsions, J. Mater. Chem. A. 6 (2018) 24641–24650. https://doi.org/10.1039/c8ta10071c.

[24] C. Liu, D. Saeki, L. Cheng, J. Luo, H. Matsuyama, Polyketone-based membrane support improves the organic solvent resistance of laccase catalysis, J. Colloid Interface Sci. 544 (2019) 230–240. https://doi.org/10.1016/j.jcis.2019.03.003.

[25] M. Yasukawa, S. Mishima, M. Shibuya, D. Saeki, T. Takahashi, T. Miyoshi, H. Matsuyama, Preparation of a forward osmosis membrane using a highly porous polyketone microfiltration membrane as a novel support, J. Membr. Sci. 487 (2015) 51–59. https://doi.org/10.1016/j.memsci.2015.03.043.

[26] L.F. Fang, L. Cheng, S. Jeon, S.Y. Wang, T. Takahashi, H. Matsuyama, Effect of the supporting layer structures on antifouling properties of forward osmosis membranes in AL-DS mode, J. Membr. Sci. 552 (2018) 265–273. https://doi.org/10.1016/j.memsci.2018.02.028.

[27] M. Yasukawa, S. Mishima, Y. Tanaka, T. Takahashi, H. Matsuyama, Thin-film composite forward osmosis membrane with high water flux and high pressure resistance using a thicker void-free polyketone porous support, Desalination. 402 (2017) 1–9. https://doi.org/10.1016/j.desal.2016.09.017.

[28] Y. Sun, L. Cheng, T. Shintani, Y. Tanaka, T. Takahashi, T. Itai, S. Wang, L. Fang, H. Matsuyama, Development of High-Flux and Robust Reinforced Aliphatic Polyketone Thin-Film Composite Membranes for Osmotic Power Generation: Role of Reinforcing Materials, Ind. Eng. Chem. Res. 57 (2018) 13528–13538. https://doi.org/10.1021/acs.iecr.8b03392.

[29] J.A. Idarraga-Mora, D.A. Ladner, S.M. Husson, Thin-film composite membranes on polyester woven mesh with variable opening size for pressure-retarded osmosis, J. Membr. Sci. 549 (2018) 251–259. https://doi.org/10.1016/j.memsci.2017.12.023.

[30] C.M. Hansen, Hansen Solubility Parameters: A Users Handbook, Second Edition, 2007. https://doi.org/10.1201/9781420006834.

[31] T. Yasui, E. Kamio, H. Matsuyama, Tough and stretchable inorganic/organic double network ion gel containing gemini-type ionic liquid as a multiple hydrogen bond cross-linker, RSC Adv. 9 (2019) 11870–11876. https://doi.org/10.1039/c9ra01790a.

[32] M. Xie, W.E. Price, L.D. Nghiem, M. Elimelech, Effects of feed and draw solution temperature and transmembrane temperature difference on the rejection of trace organic contaminants by forward osmosis, J. Membr. Sci. 438 (2013) 57–64. https://doi.org/10.1016/j.memsci.2013.03.031.

[33] S.S. Manickam, J.R. McCutcheon, Model thin film composite membranes for forward

osmosis: Demonstrating the inaccuracy of existing structural parameter models, J. Membr. Sci. 483 (2015) 70–74. https://doi.org/10.1016/j.memsci.2015.01.017.

[34] M. Park, J.J. Lee, S. Lee, J.H. Kim, Determination of a constant membrane structure parameter in forward osmosis processes, J. Membr. Sci. 375 (2011) 241–248. https://doi.org/10.1016/j.memsci.2011.03.052.

[35] A.K. Ghosh, E.M.V. Hoek, Impacts of support membrane structure and chemistry on polyamide-polysulfone interfacial composite membranes, J. Membr. Sci. 336 (2009) 140–148. https://doi.org/10.1016/j.memsci.2009.03.024.

[36] J. Kim, D.I. Kim, S. Hong, Analysis of an osmotically-enhanced dewatering process for the treatment of highly saline (waste)waters, J. Membr. Sci. 548 (2018) 685–693. https://doi.org/10.1016/j.memsci.2017.10.048.

[37] N. Togo, K. Nakagawa, T. Shintani, T. Yoshioka, T. Takahashi, E. Kamio, H. Matsuyama, Osmotically Assisted Reverse Osmosis Utilizing Hollow Fiber Membrane Module for Concentration Process, Ind. Eng. Chem. Res. 58 (2019) 6721–6729. https://doi.org/10.1021/acs.iecr.9b00630.

[38] C. Liu, R. Takagi, T. Shintani, L. Cheng, K.L. Tung, H. Matsuyama, Organic Liquid Mixture Separation Using an Aliphatic Polyketone-Supported Polyamide Organic Solvent Reverse Osmosis (OSRO) Membrane, ACS Appl. Mater. Interfaces. 12 (2020) 7586–7594. https://doi.org/10.1021/acsami.9b21519.